

GRU-TV: Time- and velocity-aware GRU for patient representation on multivariate clinical time-series data

Ningtao Liu^{1,2}, Ruoxi Gao³, and Shuiping Gou^{1,*}

¹Key Laboratory of Intelligent Perception and Image Understanding of Ministry of Education, School of Artificial Intelligence, Xidian University, Xi'an 710071, China

nt_liu@stu.xidian.edu.cn

²Robarts Research Institute, Western University, London, ON, Canada, N6A 5B7

nliu258@uwo.ca

³Electrical Engineering and Computer Science Department, University of Michigan, Ann Arbor, MI, 48109

gruoxi@umich.edu

*Corresponding author

**These authors contributed equally: Ningtao Liu, Ruoxi Gao

Abstract

Electronic health records (EHRs) are usually highly dimensional, heterogeneous, and multimodal. Besides, the random recording of clinical variables results in high missing rates and uneven time intervals between adjacent records in the multivariate clinical time-series data extracted from EHRs. Current works using clinical time-series data for patient representation regard the patients' physiological status as a discrete process described by sporadically collected records. However, changes in the patient's physiological condition are continuous and dynamic processes. The perception of time and velocity of change is crucial for patient representation learning.

In this study, we propose a time- and velocity-aware gated recurrent unit model (GRU-TV) for patient representation learning of clinical multivariate time-series data in a time-continuous manner. The neural ordinary differential equations (ODEs) and velocity perception mechanism are applied to perceive the time interval between adjacent records and changing rate of the patient's physiological status, respectively. Our experiments on two real clinical EHR datasets (PhysioNet2012, MIMIC-III) establish that GRU-TV is a robust model on computer-aided diagnosis (CAD) tasks, especially on sequences with high-variance time intervals.

INTRODUCTION

In recent years, a large number of health care-relevant records [10] are used for computational analysis. According to the Healthcare Cost and Utilization Project (HCUP) of the National Inpatient Sample, in 2018, more than 7 million patients in the United States were hospitalized, and over 10 million medical records are generated¹. Clinician decisions on treatment and diagnosis of diseases highly rely on these medical records, such as lab tests, previous procedures, medications, and diagnoses. A large amount of clinical data provide an opportunity for computer-assisted diagnosis (CAD) applications, specifically those with machine learning methods.

Recently, there are researchers focused on clinical diagnosis tasks using patient representation learning, such as patient subtyping [1, 3, 28], mortality prediction [11, 21, 26, 27], length-of-stay prediction [20, 21, 26], 24-hour decomposition [21, 24, 26], and multi-task learning [8].

RNN and its variant models such as long short term memory (LSTM), and gated recurrent unit (GRU) are widely used for patient representation learning with time-series data in these previous studies. However, multivariate sequences extracted from electronic health records (EHRs) are usually high-dimensional, heterogeneous, and multimodal [19], since the data points in EHRs are typically collected from different resources, including medical sensors and medical laboratories. In addition, the missing rate of variable values is high in these sequences, which results in an irregular missing pattern. Multiple sources and a high missing rate lead to uneven time intervals between records in the sequence. These properties result in basic RNNs that do not work well for patient representation learning because the basic assumptions of RNNs are that the time interval between records in the input sequence is uniform and the length of the records is consistent.

Improved RNN models [1, 25] adapt to clinical time-series data by integrating time intervals into the model. These methods require nonlinear mapping of time intervals and represent the patient's physiological state in a discrete manner. The RNNs with decay term present in [2, 4] decay the hidden state in forward propagation by the time decay terms, which was proven not to improve performance over standard RNN in [14]. In addition to improving the basic RNN units, some methods applied ordinary differential equation (ODE) to RNN for processing non-uniformly sampled time-series data [7, 18] after the neural ODE was proposed in [6].

In clinical practice, instantaneous vital sign rate related to physiological dynamics is an important indicator of the human health condition [29]. Thus, the perception of changes in a patient's physical condition is also critical for patient representation learning. Current RNN models, whether rep-

¹<https://www.hcup-us.ahrq.gov/db/nation/nis/nissummstats.jsp>

representing a patient’s physiological status in a continuous or discrete manner, lack the ability to perceive the changes in patient’s physiological status.

In this work, we propose a Time- and Velocity-aware GRU (GRU-TV) for patient representation based on GRU. In the proposed GRU-TV, the update of the hidden state and the forward propagation of the RNN along time are parallel, which interacts through the ODE of the hidden state and the time interval. Inspired by neural ODE, the forward propagation of hidden states between records is improved to perceive the time interval. Besides, the velocity perceptron is achieved by expanding the instantaneous rate of the hidden state into the gate.

RELATED WORK

Related works using deep learning models for patient representation learning, such as length of stay prediction [17], in-hospital mortality prediction [12], patient phenotyping [1], and international classification of diseases (ICD) code classification [16] follow a similar paradigm. In this paradigm, the deep learning models are used for representing a patient’s physiological condition and are followed a task-specific network for generating specific predictions or classification results. Therefore, the design of a deep learning model for patient representation based on EHR is critical for performance. In this section, we review related work from two perspectives, patient representation learning and time interval perception.

Patient representation learning. In terms of methods, deep learning models are increasingly used in patient representation learning tasks. These models are generally generic, i.e., task-independent, focusing on the representation of the patient’s physiological condition from clinical time-series data extracted from the EHR. Many studies have applied different methods on the basic RNN model to adapt to the sparsity, high dimensionality and inhomogeneity of clinical time series data. L Lei et al. applied a recurrent neural network and autoencoder to encode a patient’s hospital records into a low-dimensional dense vector [12]. Considering the varying length of patients’ EHRs, the non-negative tensor factorization models the input sequence to a temporal tensor and serves as the input to the LSTM [27]. In addition to RNNs, convolutional neural networks (CNNs) are also used for patient representation learning tasks. Compared with RNN, CNN cannot handle sequence data of indefinite length, so the sequence needs to be preprocessed before being input to the CNN. In [23], the patient visit sequence data is used as input to the CNN after being padded to a fixed length, while in [26], CNN is used to extract features from the dense ECG waveform and as part of the input to the RNN model. The above deep learning models can be followed by task-specific output layers for various clinical tasks, such as mortality prediction [17], length-of-stay prediction [30], patient subtyping [1], medical cost [22] etc.

Perception of uneven time intervals The uneven time interval between two adjacent records in the time-series sequence is a typical characteristic of clinical multivariate sequences. The uneven time interval results from differences

in data modality (e.g., waveform data, the medical prescription text, manual record, and medical examination result values) and their observation frequency. However, Basic RNN cannot be used to perceive uneven time intervals between input records since the time interval between records in the sequence and the changing rates of the variables are assumed to be consistent by default. Based on the assumption that the longer the time interval, the lower the reliability of the memory inherited by the RNN from the previous moment, T-LSTM [1] uses the time interval between adjacent records after a nonlinear mapping (monotonically decreasing function) as a discounting factor for the short-term memory of the previous timestep accepted by the LSTM unit. In DeepCare [15], time parameterization is introduced to handle irregular timing by modifying the forget gate. Signe Moe et al. [13] shows another route to improve the forward propagation between adjacent units of the RNN along the neural ODE proposed in [5] so that it possesses the ability to perceive uneven time intervals between records in a sequence.

The changing rate of variables in real-world data, especially in clinical scenarios, is also an important consideration for making correct decisions. The above studies have attempted to improve the basic RNN and thus deal with the time interval in the sequence, but have not yet aimed at directly sensing the rate of change in physiological conditions.

DATA DESCRIPTION

Medical time-series data from EHR contain multiple variables to describe the physiological status of the patients with different dimensions, and more abundance in types and modalities of clinical variables in the intensive care unit (ICU). The way these variables are obtained is highly variable, i.e., the sampling frequencies of waveform data (e.g. electrocardiogram) are higher than 30 Hz, blood gases (e.g., oxygen saturation, partial pressure of oxygen) are often performed every 10 minutes, vital signs (heart rate, pH, and respiratory rate) are performed every 5 minutes, respectively, and demographic information (e.g., height, gender, and age) are recorded only once during an admission. Furthermore, manual recording often causes random missing variables.

As shown in Figure 1 for an ICU stay sample extracted from MIMIC-III by pipeline provided in [8], the clinical variables in the sequence are missing to varying degrees, and even some clinical variables (e.g., FiCO_2) are completely missing. The mean and standard deviation of the missing rate for each clinical variable obtained from the statistics of all ICU stays are shown in Figure 2, in which the missing rate of these clinical variables is usually higher than 0.5, or even higher than 0.9.

Another significant characteristic is that the elapsed time between two records in the sequence is not uniform. The mean and standard deviation of the time interval between adjacent records at different sampling rates for the PhysioNet2012 and MIMIC-III datasets used in this study are shown in Figure ???. This inhomogeneity is also caused by differences in the timing and frequency of individual variable acquisitions, so aligning the values of the variables ac-

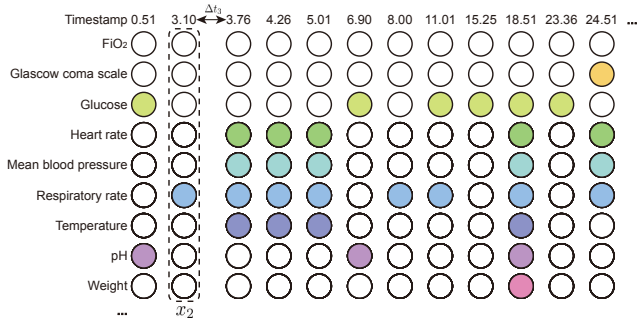


Figure 1: A sample of clinical multivariate time series data extracted from MIMIC-III. Without loss of generality, the variables and timestamps in the sequence are sampled. The colored circles indicate that the corresponding variable has a real value collected at that timestamp, while the gray circles indicate that the variable is missing. The timestamp is a relative time generated from the time the patient was admitted to the ICU as the starting time point.

ording to time manifests itself as an uneven time interval between records.

In this study, we describe a clinical time series S with a length of n as a set containing n records x , i.e., $S = \{x_1, x_2, \dots, x_n\}$, $|S| = n$. Given D_r is the dimension of time series data, record $x_i \in \mathbb{R}^{D_r}$ can be described as the set of clinical variables that are observed at the time t_i . The elapsed time between two adjacent records is defined as $\Delta t_i = t_i - t_{i-1}$, $\Delta t_1 = 1$ which is not assumed consistent in this study. The record x_{t_i} is also not assumed to contain complete clinical variables, i.e. $|x_{t_i}| \leq D_r$.

METHOD

The overall structure of GRU-TV is shown in Figure 4. It contains two main components based on GRU, which will be described below: the time interval perception to perceive the time interval between adjacent records in the sequence, and the velocity perception to perceive the velocity at which the physiological status representation of the patient corresponding to the input sequence changes. Our approach is not limited to GRU but can be applied to any RNN model and its variants as a plug-and-play plugin.

Missing value preprocessing

As mentioned in Section , there are a large number of missing value in clinical multivariate time-series data, while GRU takes fixed-length vectors as input, so data padding is widespread in this data. The missing variables in the series are filled with the latest value, that is, the actual value of the filled variable in the previous collection is used as the filling value (if the record is missing at the beginning of the series, the default value of the variable is used as the real value). However, a large number of filling values introduce noise into the input data and change the inherent distribution of the variable, so the filling values and real values should be distinguished so that the GRU can perceive the difference.

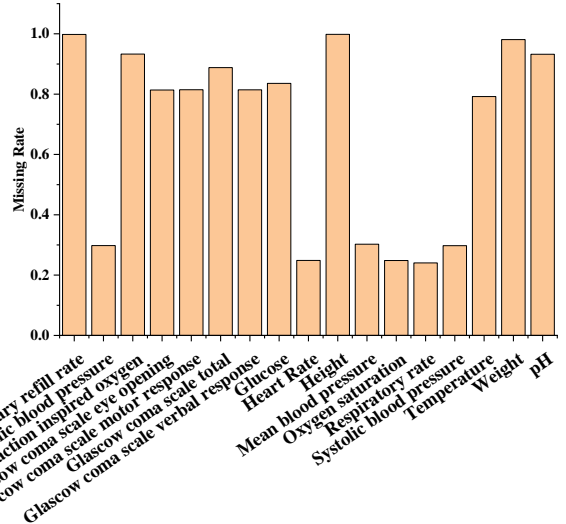


Figure 2: The missing rates of the clinical variables.

In GRU-TV, we expand the input of the basic standard GRU to include the variable mask vector corresponding to the input record as well. The forward propagation of the standard GRU is modified as follows:

$$\begin{aligned}
 r_i &= \sigma(W_r[x_i, h_{i-1}, m_i] + b_r) \\
 z_i &= \sigma(W_z[x_i, h_{i-1}, m_i] + b_z) \\
 g_i &= \tanh(W_g[x_i, r_t \odot h_{i-1}, m_i]) \\
 h_i &= z_i \odot h_{i-1} + (1 - z_i) \odot g_i
 \end{aligned} \tag{1}$$

where W_r , W_z , and $W_g \in \mathbb{R}^{(D_r \times 2 + D_h) \times D_h}$ are the weights of GRU, b_r , b_z and $b_g \in \mathbb{R}^{D_h}$ are the bias of GRU, $\sigma(\cdot)$ is sigmoid activate function, and \odot is element-wise multiplication.

Time interval perception

For a sequence with length n , RNNs such as GRU update the hidden state by combining the transformation of the previous hidden state and the current input record:

$$h_{i+1} = \text{GRU}(h_i, x_i, \theta_i) \tag{2}$$

where $i \in \{0, \dots, n\}$ and $h_i \in \mathbb{R}^{D_h}$. This transformation is discrete and does not take into account the time interval between adjacent records, and therefore has natural drawbacks for patient representation learning using multivariate clinical data. To alleviate this deficiency, we would like GRU to update the hidden state as follows:

$$h_{i+1} = \text{GRU}'(h_i, x_i, t_i, t_{i-1}, \theta_i) \tag{3}$$

where t_i and t_{i-1} are the timestamps of records x_i and x_{i-1} , respectively.

Inspired by the neural ODEs proposed in [6], instead of expanding an additional elapsed time as the input to the GRU cell, we keep the forward propagation of the standard GRU cell unchanged in this step but improve the update method of the hidden state h_t after the cell receives a record.

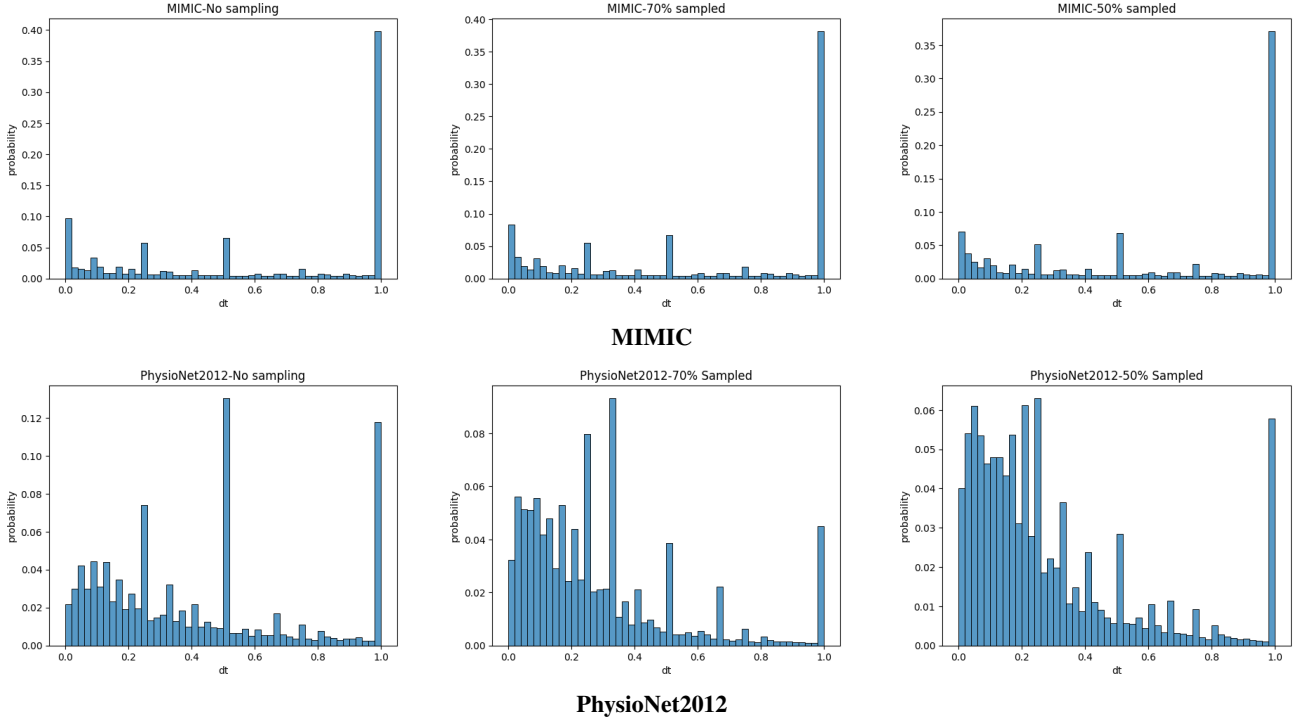


Figure 3: Time Interval Distribution

In the proposed GRU-TV, the hidden representation h_n is not fed into GRU directly in the next timestep, but we obtain the differential equation for h_t :

$$\begin{aligned} \Delta h_i &= h_i - h_{i-1} \\ &= (1 - z_i) \cdot (g_i - h_{i-1}) \end{aligned} \quad (4)$$

which leads to the update of h_i

$$h_i = h_{i-1} + \Delta t_i \cdot \Delta h_i \quad (5)$$

where $\Delta t_i = t_i - t_{i-1}$ is the elapsed time of x_i and x_{i-1} .

Velocity perception

In clinical practice, the instantaneous rate of vital signs associated with physiological kinetics is an important indicator of a patient’s physiological status. How to parameterize the instantaneous rate of a patient’s physical condition by GRU? In the proposed GRU-TV, the ODE of the hidden state is also used as an input thus giving the GRU the ability to perceive the velocity. As proved in [6, 7], when the time interval between adjacent records is infinitesimal, the limiting form of the hidden state in Section , i.e., its ODE is:

$$\frac{dh(t)}{dt} = (1 - z(t)) \cdot (g(t) - h(t)) \quad (6)$$

The ODE of h_t stays within the $[-1, 1]$ range, which guarantees the convergence of our model.

Although the instantaneous rate of h exists, we still use its discrete form as an input to GRU in this study for computa-

tional convenience:

$$\begin{aligned} r_i &= \sigma(W_r[x_i, h_{i-1}, m_i, \Delta h_i] + b_r) \\ z_i &= \sigma(W_z[x_i, h_{i-1}, m_i, \Delta h_i] + b_z) \\ g_i &= \tanh(W_g[x_i, r_i \odot h_{i-1}, m_i, \Delta h_i] + b_g) \\ \Delta h_i &= (1 - z_i) \cdot (g_i - h_{i-1}) \\ h_i &= h_{i-1} + (t_i - t_{i-1}) \cdot \Delta h_i \end{aligned} \quad (7)$$

where $\Delta h_i \in \mathbb{R}^{D_h}$ is the discrete form of dh , which is defined earlier, W_r , W_z , and $W_g \in \mathbb{R}^{(D_r \times 2 + D_h \times 2) \times D_h}$ are the weight.

It is worth noting that here we use the instantaneous rate of the hidden state rather than the input variable as the velocity for the perception module. The reason is that the velocity of the input variable cannot be accurately obtained because there are a large number of filled values in input sequence, while the hidden state can better represent the patient’s physiological condition.

Loss function

The hidden attitudes obtained after traversing the entire input sequence are fed into a task-specific separator, which in this study is a fully-connected neural network with a sigmoid function as the activation function. Binary cross entropy loss (BCE) loss was selected as the loss function since the experiments in this study are multi-label binary classification tasks. The BCE loss is defined as:

$$\mathcal{L} = \frac{1}{K} \sum_{k=1}^K y_k \cdot \log(\hat{y}_k) + (1 - y_k) \cdot \log(1 - \hat{y}_k) \quad (8)$$

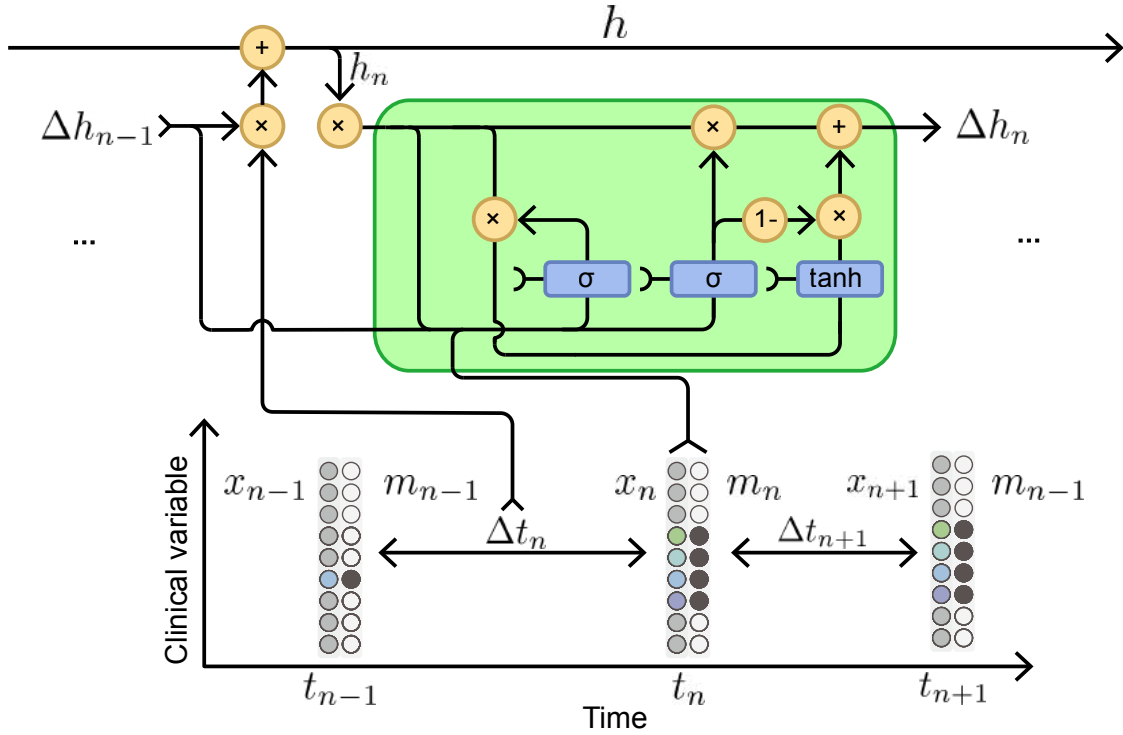


Figure 4: Illustration of GRU-TV Unit

where $y_k \in \{0, 1\}$ is the label of k^{th} binary classification task, and $\hat{y} \in (0, 1)$ is the predicted probability of k -th classification task.

Sequence sampling

The scale of sequential sampling is record, i.e., for each time series in the dataset, a certain percentage of records are selected to construct the post-sampling time series. In this study, two sequence sampling methods are applied to verify the performance of the algorithm on data sets with uneven time intervals. Native random sampling was applied to the Physionet2012 dataset. Any record in the sequence was selected with equal probability because of the uniform distribution of time intervals between the adjacent records. As shown in the figure, the most time intervals between adjacent records are 1 hour in MIMICIII dataset. An inverse proportional sampling method shown in Algorithm ?? was applied so that the time interval between adjacent records can be evenly distributed.

In Algorithm ??, the sampling scale dictionary P is generated as follows:

$$p_t = \frac{1}{c_t \times C_{all}} \quad (9)$$

$$C_{all} = \sum_{t \in \omega} c_t$$

where p_t is the probability that the record with time interval t from the previously selected record is selected, c_t is the

number of time intervals t between adjacent records in the original dataset. Fewer time intervals in the original dataset are more likely to be sampled. Sampling stops when the rate of sampled records to the records in the original data set reaches the target rate.

EXPIREMENT

Comparing model

We compare our proposed method to the following deep learning methods: GRU-Standard, GRU-Decay [4], LSTM [9], and T-LSTM [1]. We also take the only-time-aware included model (GRT-T) as a comparison model and the γ_h and γ_x used in GRU-Decay are also embedded in GRU-T respectively for more comprehensive comparisons. For GRU-T- γ_h , the h_i calculated in Equation 1 is modified by γ_h :

$$\gamma_{h_i} = e^{\{-\max(0, W_{\gamma_h} \delta_t + b_{\gamma_h})\}} \quad (10)$$

$$h_i \leftarrow h_i \gamma_{h_i}$$

where δ_t is a vector containing the elapsed time of the last collection for every variable. For GRU-T- γ_x , the trainable decay coefficient is applied in the filling of the missing values in record x_t :

$$\gamma_{x_i} = e^{\{-\max(0, W_{\gamma_x} \delta_t + b_{\gamma_x})\}}$$

$$\hat{x}_t^d = m_i^d x_i^d + (1 - m_i^d) (\gamma_{x_i}^d x_{last}^d + (1 - \gamma_{x_i}^d) \tilde{x}^d) \quad (11)$$

where \tilde{x}^d is the default value of d -th (the average of real value is used as default in this study). For GRU-T- γ_{h+x} , both

Algorithm 1: Inverse proportional sequence sampling

```
input : Sampling probability dictionary:  
         $P = \langle t, p_t \rangle$ ,  
        Sequence dataset:  $D = S$ ,  
        Target sample rate:  $T$   
output: Selected index dictionary:  $I = \langle S, idx \rangle$   
1 for  $S \in D$  do  
2   |  $D[S] \leftarrow [0]$   
3 end  
4  $R \leftarrow 0$   
5 while  $R < T$  do  
6   | for  $S \in D$  do  
7     | for  $i \leftarrow 1$  to  $LEN(S)$  do  
8       | if  $i \in I[S]$  then  
9         | CONTINUE  
10        | end  
11        |  $t \leftarrow TimeInterval(S[i], I[S])$   
12        |  $p \leftarrow P[t]$   
13        |  $r \leftarrow RandomNum(0, 1)$   
14        | if  $r \leq p$  then  
15          |  $AppendIndex(I[S], i)$   
16        | end  
17      | end  
18    | end  
19    |  $R \leftarrow CalSampleRate(D, I)$   
20 end
```

the γ_h and γ_x in GRU-Decay are applied in GRU-T.

Dataset

We demonstrate the performance of our proposed models on two real-world EHR datasets: PhysioNet2012² and MIMIC-III³, and both of them are publicly available.

PhysioNet2012 is a dataset for the PhysioNet Computing in Cardiology Challenge 2012. This multivariate clinical time series dataset consists of records from 12,000 ICU stays, all patients were adults who were admitted for a wide variety of reasons to cardiac, medical, surgical, and trauma ICUs. ICU stays of less than 48 hours have been excluded from this study.

MIMIC-III is a large, freely-available dataset comprising health-related data associated with over 40,000 patients who stayed in critical care units of the Beth Israel Deaconess Medical Center between 2001 and 2012. Over 58,000 hospital admission records were collected in this dataset.

For each dataset, after organizing the sporadically recorded data points into multivariate time series S , the variable time interval sequence Δ and mask sequence M corresponding to S was obtained by referring to the pipeline in GRU-Decay [4]. In addition, the elapsed time between adjacent records x_{t_i} and $x_{t_{i-1}}$ in the elapsed time sequence required for GRU-T was obtained by the difference between

the corresponding time points t_i and t_{i-1} , where the elapsed time between x_1 and the previous record was set to 1.

Experimental Setup

To permit a fair comparison between the methods, consistent hyperparameters, network setting, training pipeline, and dataset splits were used for all the deep learning methods. The training was stopped if the training epoch is greater than 30 and there is no performance improvement on the validation set for 3 consecutive iterations. The parameters with the best validation performance were selected to evaluate the performance on the test dataset. The final performance was the average of three independent test performances. The comparison metric for this study was the area under the ROC curve (AUROC). The macro average AUC was also calculated for the multi-task classification.

The hidden states, obtained after traversing all records in the input sequence, are fed to a fully connected layer to obtain predictions. The sigmoid activation function was used for multi-label binary classification.

In this study, the current optimal models GRU, GRU-Decay and T-LSTM, which are widely used for patient representation learning using clinical sequences, are used as comparison models. Furthermore, ablation experiments are also conducted to evaluate the performance improvement of each module.

Multi-task classification on PhysioNet2012

In this study, PhysioNet2012 dataset was used for multi-task classification, which contains four sub-tasks: in-hospital mortality prediction, length-of-stay classification, cardiac condition classification, and surgery recovery prediction.

In this task, the non-sequential variables in the dataset were discarded due to the basic GRU unit requires the input of sequence data. The variables of the time series were reorganized, in which variables collected at the same point in time or those collected at intervals of less than 5 minutes were aligned in the same record.

Table 1 depicts the experimental results on the multi-task classification of PhysioNet2012 dataset. For each metric, the best and second best are marked in bold and underlined, respectively.

In general, the application of ODE improves the performance of the standard GRU for each subtask, and this improvement is more obvious in the sampled simulation data. The velocity perception was more significant for performance improvement compared to time interval perception, especially on sampled datasets.

When the full sequences are used, The GRU-T model combined with γ_h term or γ_x term performs best on in-hospital mortality and length-of-stay less than 3 days prediction tasks, while on cardiac and surgery classification tasks, GRU-Decay performs better. In terms of average performance, GRU-T combined with γ_h term and GRU-T are optimal and sub-optimal models, respectively. When simply comparing GRU-T and GRU-Decay, the former has a more pronounced improvement relative to the GRU-Standard model. The velocity perception module of GRU-

²<https://www.physionet.org/content/challenge-2012/1.0.0/>

³<https://mimic.mit.edu/>

Table 1: Performances comparison of methods on multi-task classification of complete PhysioNet2012 dataset, and sampled PhysioNet2012 dataset with 70% and 50% sampling rate. AUROC: area under the receiver operating characteristic curve, AUPRC: area under the precisionrecall curve, Mor: in-hospital mortality, LoS: length-of-stay less than 3 days, Car: whether the patient had a cardiac condition, Sur: whether the patient was recovering from surgery, Mac: macro average AUCROC. The best and second-best performance for each subtask as well as the average are bolded and underlined.

Sampling Rate	Method	AUROC				
		Mor	LoS	Car	Sur	Mac
100%	GRU-Standard	0.8638	0.8043	<u>0.9510</u>	0.8956	0.8787
	GRU-Decay	0.8601	0.8199	0.9525	0.9043	0.8842
	T-LSTM	0.8469	0.7639	0.9274	0.8735	0.8529
	GRU-T- γ_h	0.8641	0.8432	0.9507	0.8992	0.8893
	GRU-T- γ_x	<u>0.8667</u>	0.8200	0.9497	0.8947	0.8827
	GRU-T- γ_{h+x}	0.8864	0.8086	0.9438	0.8980	0.8842
	GRU-T	0.8619	0.8255	0.9499	0.9019	<u>0.8848</u>
	GRU-TV	0.8498	<u>0.8380</u>	0.9475	<u>0.9028</u>	0.8845
70%	GRU-Standard	0.6709	0.7254	0.9170	0.8046	0.7795
	GRU-Decay	0.6488	0.7774	0.8492	0.7461	0.7554
	T-LSTM	<u>0.7512</u>	<u>0.7924</u>	0.9097	<u>0.8215</u>	<u>0.8187</u>
	GRU-T- γ_h	0.7371	0.7808	0.8987	0.8074	0.8060
	GRU-T- γ_x	0.7085	0.7699	0.8914	0.8063	0.7940
	GRU-T- γ_{h+x}	0.7449	0.7716	0.9026	0.8005	0.8049
	GRU-T	0.7505	0.7698	<u>0.9194</u>	0.8135	0.8133
	GRU-TV	0.7891	0.8017	0.9208	0.8539	0.8413
50%	GRU-Standard	0.7132	0.7160	0.8957	0.8102	0.7838
	GRU-Decay	0.7426	0.7857	0.8819	0.8093	0.8049
	T-LSTM	0.7666	0.7082	<u>0.9133</u>	<u>0.8291</u>	0.8043
	GRU-T- γ_h	0.7425	0.7357	0.8942	0.8062	0.7946
	GRU-T- γ_x	0.7222	0.7395	0.9013	0.8026	0.7914
	GRU-T- γ_{h+x}	0.7248	<u>0.7724</u>	0.9032	0.8122	0.8031
	GRU-T	0.7453	0.7712	0.9045	0.8183	<u>0.8098</u>
	GRU-TV	0.7792	0.7683	0.9193	0.8467	0.8283

TV does not improve the performance of each subtask compared to GRU-T.

In the sampled datasets, perception of the time interval between records is more important since random sampling results in a more uneven time interval between records in a sequence. The importance of the ability to perceive the unevenness of the time interval between records can be demonstrated by the improved performance of T-LSTM and GRU-T on each subtask relative to the other models. Except for the length of stay classification subtask, the γ_h and γ_x terms in GRU-Decay can even have a negative impact on the performance whether they are applied to GRU-Standard or GRU-T.

When evaluating using the sampled datasets, GRU-TV significantly outperforms the other models in every subtask. Compared to the suboptimal models, the AUC of GRU-TV improves by 2.8% and 2.3% on 70% and 50% sampled datasets, respectively.

The average macro AUC of GRU-T and GRU-TV in the three data sets are 0.8360 and 0.8514, which are both better than the 0.8253 of T-LSTM. This shows that our proposed GRU-T and GRU-TV are generalizable and robust on both sampled and complete datasets.

Acute phenotype classification on MIMIC-III

In the ICU setting, acute illnesses with short onset cycles and diagnostic time windows are more difficult to diagnose clinically and require more rapid intervention and treatment. In this study, the proposed model is evaluated by the acute phenotype subtyping task using the MIMIC dataset. Acute and unspecified renal failure, acute cerebrovascular disease, pulmonary collapse, pneumonia, respiratory failure, septicemia, and shock are included in the acute phenotypes.

When the complete dataset is used, GRU-Decay always performs best both on individual subtasks and overall performance. However, GRU-Decay's γ_h and γ_x terms applied to GRU-T can not improve the performance but have a negative effect.

On the 20% sampled dataset, the reduction in performance of the models is not significant, despite the fact that only 20% of the records are used for patient representation learning. Among them, the macro AUC of the GRU-Decay model decreased from 0.8137 to 0.7664 (5.81% reduction), while the macro AUC of the GRU-TV model decreased from 0.8050 to 0.7800 (3.11% reduction). GRU-TV is also significantly more robust than GRU-Decay on each subtask.

PATIENT REPRESENTATION

As shown in Figure 5, TODO

CONCLUSION

In this study, we proposed a GRU variant unit for modeling clinical multivariate time-series data, called GRU-TV. GRU-TV improves the forward propagation between adjacent GRUs through the ODE and velocity of the hidden state to represent the changing process of the patient's physiological status in a continuous manner.

Compared to RNN models such as GRU and LSTM, GRU-TV allows the time interval between records of the input sequence to be of free length, and eliminating the need for imputation. GRU-TV achieves state-of-the-art results on multiple tasks on both real-world datasets, especially on sampled simulated data.

The experimental results show that the proposed GRU-TV model is more advantageous in sequences with uneven time intervals, which makes GRU-TV more suitable for applications with low frequency and unstable sampling scenarios. Furthermore, the ODE and velocity representation of the hidden state in GRU-TV can be used as a plug-and-play plugin for other RNN models and achieve performance improvement. In our future work, it will be applied to other specific tasks of patient representation with clinical time-series data, to embed it in online real-time alert systems to improve computer-aided diagnostics, and to evaluate the generalizability of our model with real-world data.

ACKNOWLEDGMENT

*

Table 2: Performances comparison of acute phenotype classification using complete sequences, and sampled sequences with 70% and 50% sampling rate extracted from MIMIC-III dataset. AURF: acute and unspecified renal failure, ACD: acute cerebrovascular disease, PC: pulmonary collapse, PN: pneumonia RF: respiratory failure, SE: septicemia, SH: shock. The best and second-best performance for each subtask as well as the average are bolded and underlined.

Sampling Rate	Method	AUPRC							
		AURF	ACD	PC	PN	RF	SE	SH	MACRO
100%	GRU-Standard	<u>0.7619</u>	0.8830	<u>0.6746</u>	0.7835	0.8710	0.8070	0.8621	<u>0.8061</u>
	GRU-Decay	0.7630	0.9050	0.6901	0.7909	0.8794	0.8098	0.8577	0.8137
	T-LSTM	0.7148	0.7945	0.6545	0.7695	0.8372	0.7931	0.8326	0.7709
	GRU-T- γ_h	0.7503	0.8544	0.6709	0.7760	0.8685	0.7930	0.8533	0.7952
	GRU-T- γ_x	0.7233	0.8317	0.6530	0.7656	0.8517	0.7821	0.8340	0.7774
	GRU-T- γ_{h+x}								
	GRU-T	0.7567	0.8717	0.6726	<u>0.7892</u>	0.8733	0.8052	0.8582	0.8039
GRU-TV	0.7577	0.8817	0.6704	0.7835	<u>0.8747</u>	<u>0.8073</u>	<u>0.8598</u>	0.8050	
20% (new method)	GRU-Standard								
	GRU-Decay	0.7162	0.8040	0.6530	0.7637	0.8394	0.772	0.8169	0.7664
	T-LSTM								
	GRU-T- γ_h								
	GRU-T- γ_x								
	GRU-T- γ_{h+x}								
	GRU-T								
GRU-TV	0.7278	0.8469	0.6624	0.7689	0.8458	0.7747	0.8334	0.7800	

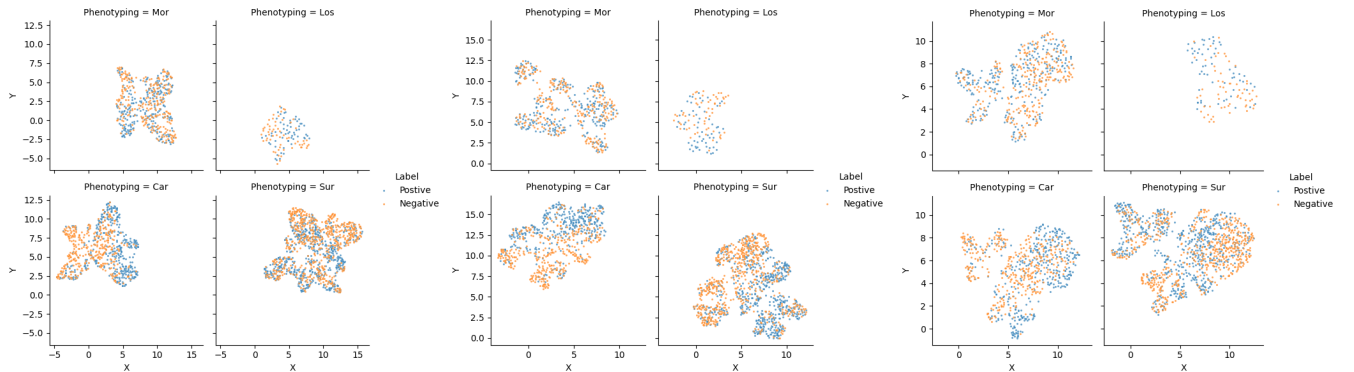


Figure 5: The UMAP Visualizations of Patient Representation

References

- [1] Baytas, I. M.; Xiao, C.; Zhang, X.; Wang, F.; Jain, A. K.; and Zhou, J. 2017. Patient subtyping via time-aware lstm networks. In *Proceedings of the 23rd ACM SIGKDD international conference on knowledge discovery and data mining*, 65–74. (document), 20
- [2] Cao, W.; Wang, D.; Li, J.; Zhou, H.; Li, L.; and Li, Y. 2018. Brits: Bidirectional recurrent imputation for time series. *Advances in neural information processing systems* 31. (document)
- [3] Che, Z.; Kale, D.; Li, W.; Bahadori, M. T.; and Liu, Y. 2015. Deep computational phenotyping. In *Proceedings of the 21th ACM SIGKDD International Conference on Knowledge Discovery and Data Mining*, 507–516. (document)
- [4] Che, Z.; Purushotham, S.; Cho, K.; Sontag, D.; and Liu, Y. 2018. Recurrent neural networks for multivariate time series with missing values. *Scientific reports* 8(1): 1–12. (document), 20, 20
- [5] Chen, R. T.; Rubanova, Y.; Bettencourt, J.; and Duvenaud, D. K. 2018. Neural ordinary differential equations. *Advances in neural information processing systems* 31. (document)
- [6] Chen, R. T. Q.; Rubanova, Y.; Bettencourt, J.; and Duvenaud, D. K. 2018. Neural Ordinary Differential Equations. In *Advances in Neural Information Processing Systems*, volume 31. Curran Associates, Inc. (document)
- [7] De Brouwer, E.; Simm, J.; Arany, A.; and Moreau, Y. 2019. Gru-ode-bayes: Continuous modeling of sporadically-observed time series. *arXiv preprint arXiv:1905.12374*. (document)
- [8] Harutyunyan, H.; Khachatrian, H.; Kale, D. C.; Ver Steeg, G.; and Galstyan, A. 2019. Multitask learning and benchmarking with clinical time series data. *Scientific data* 6(1): 1–18. (document)
- [9] Hochreiter, S.; and Schmidhuber, J. 1997. Long short-term memory. *Neural computation* 9(8): 1735–1780. 20
- [10] Johnson, A. E.; Pollard, T. J.; Shen, L.; Li-Wei, H. L.; Feng, M.; Ghassemi, M.; Moody, B.; Szolovits, P.; Celi, L. A.; and Mark, R. G. 2016. MIMIC-III, a freely accessible critical care database. *Scientific data* 3(1): 1–9. (document)
- [11] Kemp, J.; Rajkomar, A.; and Dai, A. M. 2019. Improved Hierarchical Patient Classification with Language Model Pretraining over Clinical Notes. *arXiv preprint arXiv:1909.03039*. (document)
- [12] Lei, L.; Zhou, Y.; Zhai, J.; Zhang, L.; Fang, Z.; He, P.; and Gao, J. 2018. An effective patient representation learning for time-series prediction tasks based on EHRs. In *2018 IEEE International Conference on Bioinformatics and Biomedicine (BIBM)*, 885–892. IEEE. (document)
- [13] Moe, S.; and Sterud, C. 2021. Decoupling dynamics and sampling: RNNs for unevenly sampled data and flexible online predictions. In *Learning for Dynamics and Control*, 943–953. PMLR. (document)
- [14] Mozer, M. C.; Kazakov, D.; and Lindsey, R. V. 2017. Discrete event, continuous time rnns. *arXiv preprint arXiv:1710.04110*. (document)
- [15] Pham, T.; Tran, T.; Phung, D.; and Venkatesh, S. 2016. Deepcare: A deep dynamic memory model for predictive medicine. In *Pacific-Asia conference on knowledge discovery and data mining*, 30–41. Springer. (document)
- [16] Purushotham, S.; Meng, C.; Che, Z.; and Liu, Y. 2018. Benchmarking deep learning models on large healthcare datasets. *Journal of biomedical informatics* 83: 112–134. (document)
- [17] Rajkomar, A.; Oren, E.; Chen, K.; Dai, A. M.; Hajaj, N.; Hardt, M.; Liu, P. J.; Liu, X.; Marcus, J.; Sun, M.; et al. 2018. Scalable and accurate deep learning with electronic health records. *NPJ Digital Medicine* 1(1): 1–10. (document)
- [18] Rubanova, Y.; Chen, R. T.; and Duvenaud, D. K. 2019. Latent ordinary differential equations for irregularly-sampled time series. *Advances in neural information processing systems* 32. (document)
- [19] Si, Y.; Du, J.; Li, Z.; Jiang, X.; Miller, T.; Wang, F.; Jim Zheng, W.; and Roberts, K. 2021. Deep Representation Learning of Patient Data from Electronic Health Records (EHR): A Systematic Review. *Journal of Biomedical Informatics* 115: 1–47. (document)
- [20] Si, Y.; and Roberts, K. 2019. Deep patient representation of clinical notes via multi-task learning for mortality prediction. *AMIA Summits on Translational Science Proceedings 2019*: 779. (document)
- [21] Song, H.; Rajan, D.; Thiagarajan, J.; and Spanias, A. 2018. Attend and diagnose: Clinical time series analysis using attention models. In *Proceedings of the AAAI Conference on Artificial Intelligence*, volume 32. (document)
- [22] Stojanovic, J.; Gligorijevic, D.; Radosavljevic, V.; Djuric, N.; Grbovic, M.; and Obradovic, Z. 2016. Modeling healthcare quality via compact representations of electronic health records. *IEEE/ACM transactions on computational biology and bioinformatics* 14(3): 545–554. (document)
- [23] Suo, Q.; Ma, F.; Yuan, Y.; Huai, M.; Zhong, W.; Gao, J.; and Zhang, A. 2018. Deep patient similarity learning for personalized healthcare. *IEEE transactions on nanobioscience* 17(3): 219–227. (document)
- [24] Suresh, H.; Gong, J. J.; and Guttag, J. V. 2018. Learning tasks for multitask learning: Heterogenous patient populations in the icu. In *Proceedings of the 24th ACM SIGKDD International Conference on Knowledge Discovery & Data Mining*, 802–810. (document)

- [25] Wang, T.; Qiu, R. G.; and Yu, M. 2018. Predictive modeling of the progression of Alzheimer’s disease with recurrent neural networks. *Scientific reports* 8(1): 1–12. (document)
- [26] Xu, Y.; Biswal, S.; Deshpande, S. R.; Maher, K. O.; and Sun, J. 2018. Raim: Recurrent attentive and intensive model of multimodal patient monitoring data. In *Proceedings of the 24th ACM SIGKDD international conference on Knowledge Discovery & Data Mining*, 2565–2573. (document)
- [27] Yin, K.; Qian, D.; Cheung, W. K.; Fung, B. C.; and Poon, J. 2019. Learning phenotypes and dynamic patient representations via rnn regularized collective non-negative tensor factorization. In *Proceedings of the AAAI Conference on Artificial Intelligence*, volume 33, 1246–1253. (document)
- [28] Zhang, Y.; Zhou, H.; Li, J.; Sun, W.; and Chen, Y. 2018. A Time-Sensitive Hybrid Learning Model for Patient Subgrouping. In *2018 International Joint Conference on Neural Networks (IJCNN)*, 1–8. IEEE. (document)
- [29] Zhao, H.; Hong, H.; Sun, L.; Li, Y.; Li, C.; and Zhu, X. 2017. Noncontact physiological dynamics detection using low-power digital-IF Doppler radar. *IEEE Transactions on Instrumentation and Measurement* 66(7): 1780–1788. (document)
- [30] Zhou, C.; Jia, Y.; Motani, M.; and Chew, J. 2017. Learning deep representations from heterogeneous patient data for predictive diagnosis. In *Proceedings of the 8th ACM International Conference on Bioinformatics, Computational Biology, and Health Informatics*, 115–123. (document)